PHYSICAL REVIEW B **86**, 201408(R) (2012)

Spin ordering in magnetic quantum dots: From core-halo to Wigner molecules

R. Oszwałdowski,[1] P. Stano,[2,3] A. G. Petukhov,[4] and Igor Žutić[1]
[1]*Department of Physics, University at Buffalo, Buffalo, New York 14260-1500, USA*
[2]*Institute of Physics, Slovak Academy of Sciences, 845 11 Bratislava, Slovakia*
[3]*Department of Physics, University of Basel, Klingelberstrasse 82, 4056 Basel, Switzerland*
[4]*Department of Physics, South Dakota School of Mines and Technology, Rapid City, South Dakota 57701, USA*
(Received 5 June 2012; published 26 November 2012)

The interplay of confinement and Coulomb interactions in quantum dots can lead to strongly correlated phases differing qualitatively from the Fermi liquid behavior. We explore how the presence of magnetic impurities in quantum dots can provide additional opportunities to study correlation effects and the resulting ordering in carrier and impurity spins. By employing exact diagonalization we reveal that seemingly simple two-carrier quantum dots lead to a rich phase diagram. We propose experiments to verify our predictions; in particular, we discuss interband optical transitions as a function of temperature and magnetic field.

DOI: 10.1103/PhysRevB.86.201408 PACS number(s): 75.50.Pp, 75.10.Lp, 75.30.Hx

With high tunability of their parameters, quantum dots (QDs) are ideal systems for exploring correlation effects.[1–4] While in three dimensions the correlation-induced Wigner crystal[5] is elusive and expected only in the limit of an extremely low carrier density,[2,6] its nanoscale analog, the Wigner molecule (WM),[2,3,7] has been observed in QDs at much higher densities.[8,9] An increase in the relative strength of Coulomb interactions qualitatively changes the liquidlike independent-particle picture to that of a WM characterized by electron localization and strong angular order.[3,7,8]

We expect that doping QDs with magnetic impurities[10–13] (typically Mn) will open unexplored opportunities to study the nanoscale correlations. Through Mn-carrier exchange interaction, the correlations can be enhanced, imprinted on Mn spins, and thus observed. Several key advances in elucidating correlations in nonmagnetic QDs have been accomplished in two-electron systems.[2,8,9,14] However, even in simple circular QDs, identification of WMs is complicated by insufficient accuracy in the treatment of correlations[2,14] and artifacts of the mean-field and Hartree-Fock approaches.[15] To understand these systems, exact diagonalization[8,9,14] is particularly suitable, corroborating analytical findings for two-electron correlations in QDs.[16,17]

Here, we generalize the exact approach[18,19] to probe the charge and spin densities of carriers as well as Mn spin ordering in magnetic QDs with two carriers (holes).[20] To elucidate the stability of the magnetic ordering, we consider different Mn doping configurations, deformation of circular QD confinement, and examine the effects of temperature T and magnetic field B.

The phase diagram in Fig. 1, for Mn-doped circular QDs, shows three magnetic ground states, to be contrasted with the spin-singlet ground state of nonmagnetic QDs.[2] The ground-state phase changes with the doping radius R_{eff} and the fraction x_{Mn} of cations replaced by Mn atoms in the QD. The carrier spin density is imprinted on Mn spins forming three patterns corresponding to two pseudosinglets (PSs) characterized by total hole spin zero, but nonzero hole spin density,[22] and a spin triplet (T); see Figs. 1(a)–1(c).

Before we provide a detailed analysis, it is instructive to view the PS state in Fig. 1(c) as a spin WM. In nonmagnetic circular QDs, their WM "dimerlike" phase[8] can be fully revealed only in the pair-correlation function.[17] However, a similar phase can be directly detected in magnetic QDs: the Mn pattern of the spin WM reflects a double-peaked hole spin density. The separation between carriers, characteristic for WMs,[2] is enhanced by doping with Mn, which provides a spin structure.

We use the total QD Hamiltonian, $\hat{H} = \hat{H}_f + \hat{H}_{\text{ex}}$, with typical two-dimensional (2D) nonmagnetic and exchange parts,[22] where

$$\hat{H}_f = \sum_{i=1,2}\left[\frac{\boldsymbol{\pi}_i^2}{2m^*} + \frac{m^*}{2}\left(\omega_x^2 x_i^2 + \omega_y^2 y_i^2\right)\right] + \frac{e^2/4\pi\epsilon}{|\mathbf{r}_1 - \mathbf{r}_2|}, \quad (1)$$

the holes are labeled by i, m^* is the effective mass, e the electron charge, and ϵ the dielectric constant. The momentum $\boldsymbol{\pi}_i$ includes the vector potential of the field $B \parallel z$.[23] The p–d exchange interaction between Mn spins and confined holes has the Ising form[24]

$$\hat{H}_{\text{ex}} = -(\beta/3)\sum_{i=1,2}\sum_{j=1}^{N}\hat{s}_{iz}\hat{S}_{jz}\,\delta(\mathbf{r}_i - \mathbf{R}_j), \quad (2)$$

because of the strong z-axis anisotropy, arising from spin-orbit interaction in 2D QDs. Here, β is the exchange constant and $\hat{s}_z$ is the heavy-hole pseudospin with projections $s_z = \pm 3/2$, while $\hat{S}_z$ are operators of the z projection of Mn spins positioned at $\mathbf{R}_j$, and N is the number of Mn spins in the dot.

Since $\hat{H}_{\text{ex}}$ does not contain spin-flip processes, the total wave function is a product of the hole and Mn spin parts. The partition function of the system can be calculated using the Gibbs canonical distribution $Z = \text{Tr}_{S_{jz}}\sum_n \exp[-E_n(\{S_{jz}\})/k_BT]$, where k_B is the Boltzmann constant. The hole eigenvalues E_n depend on N numbers S_{jz}, each $S_{jz} = -S, \ldots, S$ where $S = 5/2$ (the index n runs over hole states for fixed $\{S_{jz}\}$). To calculate Z, one would need to solve 6^N replicas of the hole Schrödinger equation, with $N \sim 10^2$–10^3.

We can overcome this obstacle of computational complexity by partitioning the dot into N_c square cells, each containing few Mn spins, and neglecting spatial variation of the two-hole

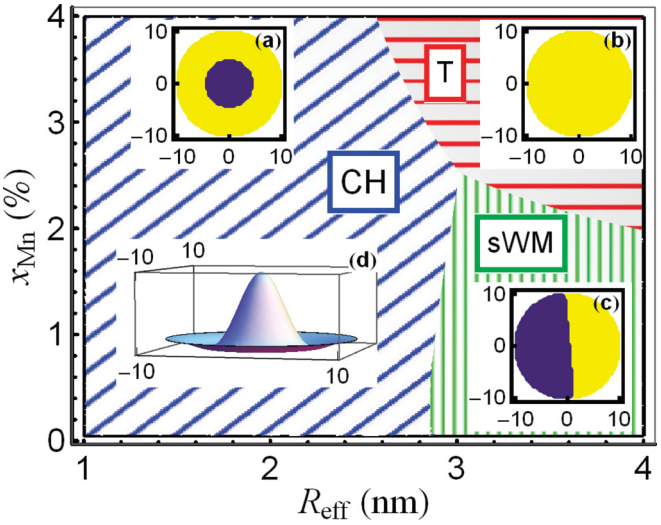

FIG. 1. (Color online) Ground-state phase diagram (PS vertical and diagonal, T horizontal hatching) as a function of Mn content x_{Mn} and Mn doping radius R_{eff}, for a double-occupied circular dot, $\hbar\omega_{x,y} = 25$ meV, at zero temperature. Insets (a)–(c): QD top view (in-plane coordinates in nanometers) of Mn spin patterns: spins up, light; down, dark. (a) Core-halo (CH), $R_{eff} = 2$ nm, $x_{Mn} = 2\%$; (b) triplet (T), $R_{eff} = 3.5$ nm, $x_{Mn} = 3\%$; (c) spin Wigner molecule (sWM), $R_{eff} = 3.5$ nm, $x_{Mn} = 1\%$; (d) hole spin density for the pattern in (a) (Ref. 21).

wave function Φ_n within each cell k through the use of the average hole spin density

$$\langle s_k\rangle_n = \frac{1}{h_z N_k}\sum_{j\in N_k}\langle\Phi_n|\sum_i \hat{s}_{iz}\,\delta(\mathbf{r}_i-\mathbf{R}_j)|\Phi_n\rangle, \qquad (3)$$

where h_z is the QD height. For a given cell with N_k spins $S_{jz}^{(k)}$ creating a magnetic moment M_k, the distribution function of the average dimensionless magnetization $m_k \equiv -M_k/g_{Mn}\mu_B N_k$ can be expressed as $Y(m_k) \propto \exp[-G_k(m_k/S)/k_BT]$. Here $g_{Mn} = 2$ is the Mn g factor. The Gibbs free energy of the N_k noninteracting spins, $G_k(m_k/S)$, is obtained by Legendre transformation,[25]

$$\frac{G_k(x)}{N_k k_B T} = \left[x B_S^{-1}(x) - \ln\frac{\sinh\left[(1+1/2S)B_S^{-1}(x)\right]}{\sinh\left[(1/2S)B_S^{-1}(x)\right]}\right], \qquad (4)$$

where B_S^{-1} is the inverse of the Brillouin function B_S. Using $Y(m_k)$, we transform Z with exponential accuracy as

$$Z \propto \sum_n \int\cdots\int \exp\left[-G_{tot}^n/k_BT\right]\prod_{k=1}^{N_c} dm_k, \qquad (5)$$

where $G_{tot}^n = \sum_k G_k(m_k/S) + E_n(\{m_k\})$. For any n, each integral in Eq. (5) can be evaluated using the steepest-descent method. The equation for the saddle point, combined with the Hellmann-Feynman theorem $-\beta N_k\langle s_k\rangle/3 + g_{Mn}N_k\mu_B B = \partial E_n(m_1,\ldots,m_k,\ldots,m_{N_c})/\partial m_k$, leads to the self-consistency condition

$$m_k = SB_S[S(\beta\langle s_k\rangle_n/3 - g_{Mn}\mu_B B)/k_BT]. \qquad (6)$$

Our analysis shows that Eq. (6) depends on the quantum-mechanical average $\langle s_k\rangle_n$ relevant for small systems such as QDs, rather than on the thermal average,[25] thereby avoiding artifacts arising from imposing the thermodynamic limit on a nanoscale system. We use Eq. (6) to find a global minimum of $G_{tot}^0(\{m_k\})$ corresponding to the ground state, where 0 stands for PS or T in different regions of the phase diagram.

We find the eigenstates of $\hat{H}$ self-consistently: For fixed values of m_k (randomly initialized), we obtain intermediate two-hole states. Since $[\hat{H},\hat{\Sigma}_z]$=0, where $\hat{\Sigma}_z$ is the total hole-spin z projection, the states are in either PS ($\Sigma_z = 0$) or T ($\Sigma_z = \pm 3$) orthogonal subspaces.[22] We choose the lowest state in each subspace, use Eq. (6) to obtain new m_k, and restart exact diagonalization, iterating until convergence. The ground-state nature, either T or PS, depends on the QD parameters (for $x_{Mn} = 0 = B$ the ground state is a singlet).

We use ZnTe parameters: hole mass $m^* = 0.2\times$ electron mass,[26] $\epsilon = 9.4\epsilon_0$,[27] with ϵ_0 the vacuum permittivity, and $N_0\beta = -1.05$ eV,[28] with the cation density $N_0 = 4/a^3$ given by the lattice constant $a \simeq 6.1$ Å. For typical self-assembled QDs, $\hbar\omega_{x,y} = 10{-}30$ meV, $x_{Mn} \leqslant 5\%$. Our standard values are $x_{Mn} = 1\%$, $h_z = 1.8$ nm, and $\hbar\omega_0 \equiv \hbar\omega_{x,y} = 25$ meV, corresponding to a characteristic length[29] $l_0 = (\hbar/m^*\omega_0)^{1/2} = 3.9$ nm.

We now reconsider the Mn patterns in Fig. 1, calculated at $T = 0$, with a doping profile $x_{Mn}\{1+\exp[(r-R_{eff})/\xi]\}^{-1}$ of width $\xi = 0.25$ nm, and radius R_{eff}; here r is the distance from the QD center. In addition to the triplet ground state (all Mn spins parallel) at relatively large R_{eff} and x_{Mn}, and the spin-WM ground state at smaller x_{Mn}, another PS forms [Fig. 1(a)], which we call the "core-halo."[30] The inset (d) shows the resulting average spin density $\langle s_k\rangle$. In contrast to the spin WM, the Mn pattern and $\langle s_k\rangle$ for the core-halo preserve the circular symmetry of the QD. For $\xi \to 0$ (no Mn for $r > R_{eff}$) and small enough R_{eff} (e.g., $R_{eff} = 2$ nm, $x_{Mn} = 1\%$) the core-halo patterns become purely "ferromagnetic." We find that such unidirectional patterns form also for other inhomogeneous x_{Mn} profiles, confirming predictions from Ref. 22.

In the $R_{eff} \to \infty$ regime, we study the stability of T and PS states, termed magnetic bipolarons.[22] Figure 2(a) shows that, already at modest x_{Mn}, the Mn-induced energy gain of PS exceeds that of a magnetic polaron forming for a single carrier.[32] This suggests that the robustness of magnetic bipolarons is similar to that of the well-established single magnetic polarons.

Figure 2 shows the temperature dependence of the bipolaron energies. Owing to the stronger exchange interaction, the triplet approaches the high-T limit at a higher T than does the PS. The asymptotic trend $-1/T$ in E_T, reminiscent of paramagnets, is expected since the effective exchange field of triplet holes, acting on Mn, is nearly independent of the Mn spin alignment. In contrast, the PS has a second-order transition to a singlet. Insets (b)–(d) show the magnetization [Eq. (6)] of the PS and T patterns. Finite temperature has a different effect on the two states. For the PS, m_k retains its overall 0 K shape, and decreases uniformly. In contrast, the saturated Mn pattern of the T [Fig. 1(b)], undergoes a transition to a state with spontaneously broken circular symmetry: two symmetrical and unidirectional peaks appear [Fig. 2(b)]. The peaks reflect the hole spin density, which maximizes the Mn-induced energy gain through a

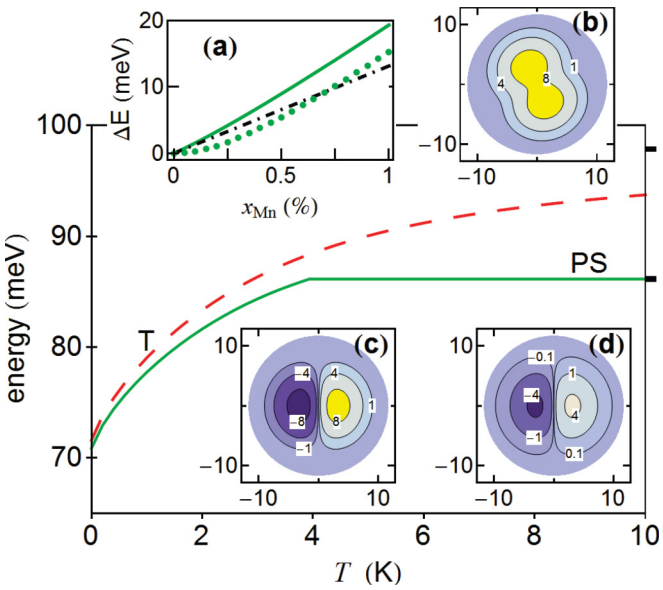

FIG. 2. (Color) Temperature evolution of pseudosinglet E_{PS} (green) and triplet E_T (red) energies for a circular QD, $\hbar\omega_{x,y} =$ 25 meV, and $x_{Mn} = 1\%$ (homogeneous distribution). Bold ticks show the high-T (zero p–d exchange) limit. (a) Mn-induced energy gains at $T = 0$ K. Dots (solid line), numerical (variational) results (Ref. 31) for the PS, $\Delta E_{PS} = E_{PS}(x_{Mn} = 0) - E_{PS}$. Dash-dotted line, single magnetic polaron, $\Delta E_{MP} = x_{Mn} N_0 |\beta| S/2$. $\Delta E_{MP} < \Delta E_{PS}$ for $x_{Mn} \geqslant 0.7\%$. Insets (b)–(d) m_k in units of 1/4 as a function of position (nm); (b) triplet at 1 K, (c), (d) PS at 1 K, 3 K.

linear combination of the two triplets with opposite angular momenta.[12]

Having established the presence of magnetic bipolarons and Mn patterns in circular QDs, it is crucial to examine the more realistic case of asymmetric confinement. We introduce in-plane asymmetry through $\omega_{x,y} = \hbar/(m^* l_{x,y}^2)$, where $l_{x,y} = l_0(1 + d)^{\pm 1}$.[33] The asymmetry stabilizes the spin WM along the weaker-potential axis, Fig. 3(a), since separating the holes in the direction of the "softer" potential costs less potential energy. As in circular QDs (Fig. 1, large R_{eff}), the triplet

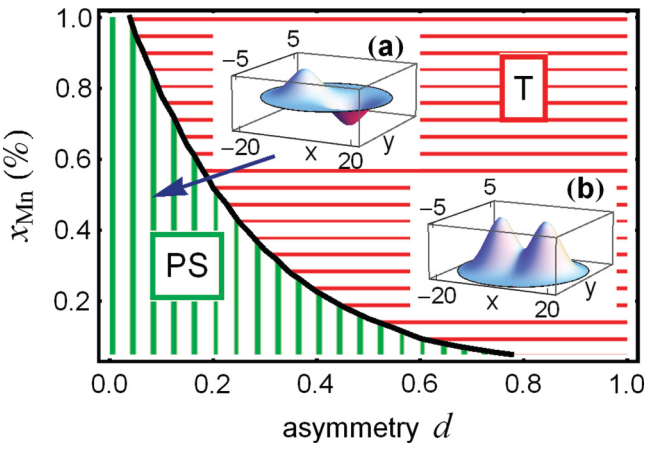

FIG. 3. (Color online) Ground-state phase diagram (PS vertical, T horizontal hatching) as a function of confinement asymmetry d and x_{Mn}, at $T = 0$. Insets: hole spin density of the PS (a) and T (b), $\hbar\omega_0 = 25$ meV, $d = 1$, and $x_{Mn} = 1\%$.

becomes the ground state with increasing x_{Mn}. For increasing asymmetry d, the nonmagnetic singlet-triplet gap decreases, so that the T becomes the ground state at lower x_{Mn}.[34]

The results so far can be understood by introducing an effective, spin-dependent interaction between the two holes. Each hole tends to polarize Mn spins within an area defined by the temperature and confinement. The consequences of the overlap of the areas depend on the relative hole spins. If they are antiparallel (PS), mutual repulsion arises,[31] which would lead to complete separation of holes in the absence of the confinement (the magnetic bipolaron would not form). In contrast, holes with parallel spins (T) effectively attract each other,[35] as they benefit from sharing the cloud of polarized Mn spins that each of them carries.[31]

Opposite limits of the doping radius R_{eff} offer a simple insight as to which of the two PS patterns is the ground state. For $R_{eff} \to 0$, the p–d exchange energy gain for the spin WM is zero, since this state produces $\langle s_k \rangle = 0$ at the QD center. On the other hand, for $R_{eff} \to \infty$ and for weak confinement, the proper limit is that of two separate, localized magnetic polarons, a scenario consistent with a spin WM rather than a core-halo.[31]

To corroborate our predictions, as well as other works considering magnetic interactions in closed-shell QDs,[13,22,36,37] we propose experiments that test the existence of magnetic bipolarons, and discriminate the different Mn patterns. One such probe is interband photoluminescence.[10,11,38] With a sufficiently intense excitation, two kinds of emission lines appear, corresponding to $2 \to 1$ and $1 \to 0$ QD occupancy transitions. We calculate the photon energies E_{ph} for the standard parameters, assuming (i) type-II band alignment,[28,31] (ii) the Mn spin pattern does not change during a recombination event, and (iii) the system recombines from its (two- or single-hole) ground state. We show that the E_{ph} dependence on T and B allows the bipolarons to be identified.

We first consider varying T (Fig. 4). A single polaron, characterized by a unidirectional Mn pattern, shows a $1/T$ redshift. In contrast, thermal disruption of the PS occurs with an abrupt change of the slope of E_{ph} at a few kelvin.

We next consider $B \parallel z$ (the Faraday configuration[28,39]). For a triplet, $m_k \parallel -B$ everywhere. The small change of ΔE_{ph} (Fig. 5, dashed line) is mainly due to orbital effects, since m_k, highly saturated at low T, is not very sensitive to B. For the PS, some of the Mn spins are aligned unfavorably, i.e., parallel to B. Increasing B changes their projection [Figs. 5(a) and 5(b)].

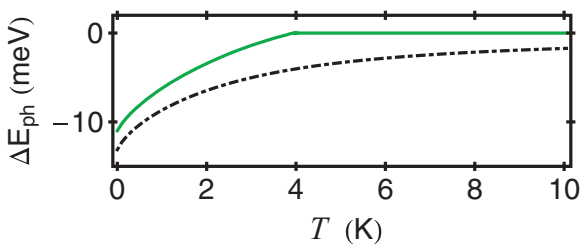

FIG. 4. (Color online) Temperature dependence of the PS $\to$ 1 hole (solid) and $1 \to 0$ (dash-dotted) transition energies E_{ph}, for $B = 0$. To better compare the dependencies, each line is shifted: $\Delta E_{ph} \equiv E_{ph}(T) - E_{ph}(T \to \infty)$. Standard QD parameters, homogeneous Mn doping.

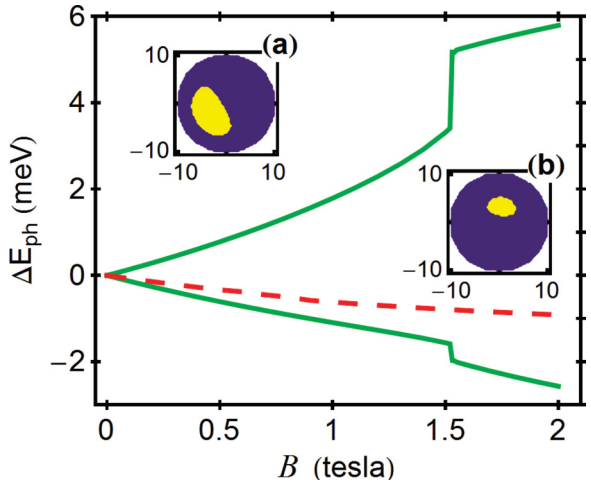

FIG. 5. (Color online) $B \parallel z$ dependence of the PS $\rightarrow$ 1 (solid lines) and T $\rightarrow$ 1 (dashed) transitions, for $T = 1$ K. To avoid PS-T crossing, we set $x_{\mathrm{Mn}} = 0.5\%$. Each line is shifted: $\Delta E_{\mathrm{ph}} \equiv E_{\mathrm{ph}}(B) - E_{\mathrm{ph}}(B = 0)$. Insets: PS Mn patterns for 0.4 (a), and 1.4 (b) tesla; light (dark) for $m_k > 0$ ($m_k < 0$).

The accompanying change of E_{PS} (not shown) becomes abrupt at a threshold B_0 (the Mn pattern becomes unidirectional at B_0), and then flattens out close to its asymptotic value: the nonmagnetic singlet energy.[40] For $B > B_0$ ($B_0 \simeq 1.5$ T in Fig. 5), the B dependence of PS $\rightarrow$ 1 transition energies is dominated by changes of final-state energies, which react to the increasing saturation of m_k. The line is split by the field, as the remaining hole can end up in two opposite-spin states. No such splitting occurs for the T $\rightarrow$ 1 and 1 $\rightarrow$ 0 transitions. Thus, the splitting and the abrupt "melting" at B_0, signal the PS ground state.

Finally, the two possible PS states can be resolved using selection rules for photoluminescence.[41] The circularly symmetric core-halo pattern forbids recombination with p-like excited electron states. However, such transitions are (weakly) allowed for the spin WM,[31] and would appear at a strong optical pumping.[42] As an alternative to photoluminescence, scanning tips with nitrogen-vacancy centers could offer sufficient spatial sensitivity to probe the Mn spin patterns.[43]

We expect that our findings will motivate efforts to probe magnetization patterns and correlation effects at the nanoscale. Previously unexplored regimes are afforded with Mn doping. Effective internal magnetic fields in colloidal QDs can reach $\sim$100 T,[11] beyond what is feasible with applied static magnetic fields. Consistent with recent advances in the field of nanomagnetism,[44] an increasing number of experimental probes are likely to meet the challenge of detecting the predicted spin ordering even in single QDs.

Nuclear spins in few-electron III-V QDs could provide a magnetically active feedback similar to that studied here. While the electron-nuclear spin interaction is weak, leading to a much smaller temperature scale for analogous polaron objects, this scale is known to be very strongly enhanced by electron-electron interactions in low-dimensional systems.[45]

This work was supported by DOE-BES, ONR, meta-QUTE ITMS NFP Grant No. 26240120022, CE SAS QUTE, EU Project Q-essence, Grant No. APVV-0646-10, and SCIEX.

[1] S. M. Reimann and M. Manninen, Rev. Mod. Phys. **74**, 1283 (2002).

[2] C. Yannouleas and U. Landman, Rep. Prog. Phys. **70**, 2067 (2007).

[3] A. Ghosal, A. D. Guclu, C. J. Umrigar, D. Ullmo, and H. U. Baranger, Nat. Phys. **2**, 336 (2006).

[4] R. Hanson *et al.*, Rev. Mod. Phys. **79**, 1217 (2007); L. P. Kouwenhoven, D. G. Austig, and S. Tarucha, Rep. Prog. Phys. **64**, 701 (2001); *Concepts in Spin Electronics*, edited by S. Maekawa (Oxford University Press, Oxford, 2006).

[5] E. Wigner, Phys. Rev. **46**, 1002 (1934).

[6] P. Fulde, *Electron Correlations in Molecules and Solids* (Springer, Berlin, 1993).

[7] R. Egger, W. Häusler, C. H. Mak, and H. Grabert, Phys. Rev. Lett. **82**, 3320 (1999).

[8] A. Singha, V. Pellegrini, A. Pinczuk, L. N. Pfeiffer, K. W. West, and M. Rontani, Phys. Rev. Lett. **104**, 246802 (2010).

[9] C. Ellenberger, T. Ihn, C. Yannouleas, U. Landman, K. Ensslin, D. Driscoll, and A. C. Gossard, Phys. Rev. Lett. **96**, 126806 (2006).

[10] J. Seufert, G. Bacher, M. Scheibner, A. Forchel, S. Lee, M. Dobrowolska, and J. K. Furdyna, Phys. Rev. Lett. **88**, 027402 (2001); L. Besombes, Y. Léger, L. Maingault, D. Ferrand, H. Mariette, and J. Cibert, *ibid.* **93**, 207403 (2004); F. Xiu *et al.*, ACS Nano **4**, 4948 (2010); S. T. Ochsenbein *et al.*, Nat. Nanotech. **4**, 68 (2009); R. Viswanatha, J. M. Pietryga, Victor I. Klimov, and S. A. Crooker, Phys. Rev. Lett. **107**, 067402 (2011); F. Henneberger and J. Puls, in *Introduction to the Physics of Diluted Magnetic Semiconductors*, edited by J. Kossut and J. A. Gaj (Springer, Berlin, 2010), Chap. 5, pp. 161–190; I. A. Merkulov and A. V. Rodina, *ibid.*, Chap. 3, pp. 65–102; Ł. Kłopotowski, L. Cywinski, P. Wojnar, V. Voliotis, K. Fronc, T. Kazimierczuk, A. Golnik, M. Ravaro, R. Grousson, G. Karczewski, and T. Wojtowicz, Phys. Rev. B **83**, 081306(R) (2011); A. A. Maksimov, G. Bacher, A. McDonald, V. D. Kulakovskii, A. Forchel, C. R. Becker, G. Landwehr, and L. Molenkamp, *ibid.* **62**, R7767 (2000); N. T. T. Nguyen and F. M. Peeters, *ibid.* **78**, 045321 (2008); J. M. Pientka, R. Oszwałdowski, A. G. Petukhov, J. E. Han, and I. Žutić, *ibid.* **86**, 161403(R) (2012); R. M. Abolfath, P. Hawrylak, and I. Žutić, Phys. Rev. Lett. **98**, 207203 (2007).

[11] R. Beaulac, L. Schneider, P. I. Archer, G. Bacher, and D. R. Gamelin, Science **325**, 973 (2009).

[12] A. O. Govorov, Phys. Rev. B **72**, 075359 (2005); C. R. Phys. **9**, 857 (2008).

[13] J. Fernández-Rossier and L. Brey, Phys. Rev. Lett. **93**, 117201 (2004); F. Qu and P. Hawrylak, *ibid.* **96**, 157201 (2006).

[14] D. Pfannkuche, V. Gudmundsson, and P. A. Maksym, Phys. Rev. B **47**, 2244 (1993).

[15] For example, the spontaneous symmetry breaking, incorrect spin configurations, and spurious radial dependence of the carrier wave function (Ref. 7) [L. Serra, R. G. Nazmitdinov, and A. Puente, Phys. Rev. B **68**, 035341 (2003)].

[16]U. Merkt, J. Huser, and M. Wagner, Phys. Rev. B **43**, 7320 (1991).
[17]M. Taut, Phys. Rev. A **48**, 3561 (1993).
[18]By systematically including the effects of carrier-Mn interactions, we generalize a method shown to be very accurate for nonmagnetic QDs [F. Baruffa, P. Stano, and J. Fabian, Phys. Rev. Lett. **104**, 126401 (2010); P. Stano and J. Fabian, *ibid.* **96**, 186602 (2006)].
[19]F. Baruffa, P. Stano, and J. Fabian, Phys. Rev. B **82**, 045311 (2010).
[20]The choice of holes, rather than electrons, leads to enhanced carrier-Mn exchange interaction. Interesting results for magnetic bipolarons based on electrons are presented in H. Bednarski and J. Spałek, J. Phys.: Condens. Matter **24**, 235801 (2012).
[21]R. Oszwałdowski, http://meetings.aps.org/link/BAPS.2012.MAR.P14.1.
[22]R. Oszwałdowski, I. Žutić, and A. G. Petukhov, Phys. Rev. Lett. **106**, 177201 (2011).
[23]The action of B on magnetic moments of holes is negligible for the effects described here.
[24]K. Vyborny, J. E. Han, R. Oszwałdowski, I. Žutić, and A. G. Petukhov, Phys. Rev. B **85**, 155312 (2012); P. S. Dorozhkin *et al.*, *ibid.* **68**, 195313 (2003).
[25]A. G. Petukhov, I. Žutić, and S. C. Erwin, Phys. Rev. Lett. **99**, 257202 (2007).
[26]Y. Oka and M. Cardona, Phys. Rev. B **23**, 4129 (1981).
[27]H. Wagner *et al.*, J. Cryst. Growth **117**, 303 (1992).
[28]I. R. Sellers *et al.*, Phys. Rev. B **82**, 195320 (2010).
[29]The importance of $x_{\mathrm{Mn}} = 0$ correlations can be estimated from the Wigner parameter $R_W = (e^2/\epsilon l_0)/\hbar\omega_0$ (Ref. 2).
[30]The actual orientations of spins in core-halo and spin-WM patterns, as well as the azimuthal angle of the division line in the latter, are not determined by $\hat{H}$, but pseudorandomly in the numerical procedure.
[31]See Supplemental Material at http://link.aps.org/supplemental/10.1103/PhysRevB.86.201408 for details.
[32]D. R. Yakovlev and W. Ossau, in *Introduction to the Physics of Diluted Magnetic Semiconductors*, edited by J. Kossut and J. A. Gaj (Springer, Berlin, 2010); T. Dietl and J. Spałek, Phys. Rev. B **28**, 1548 (1983).
[33]Equivalent to the convention from Ref. 1 and R. M. Abolfath, A. G. Petukhov, and I. Žutić, Phys. Rev. Lett. **101**, 207202 (2008).
[34]The phase boundaries (Figs. 1 and 3) result from interplay of the single-particle confinement, Coulomb interaction, and magnetic exchange. The boundaries may shift as functions of the QD parameters.
[35]S. Goupalov and A. Kavokin, Solid State Commun. **97**, 77 (1996).
[36]M. V. Milovanović, E. Dobardžić, and Z. Radović, Phys. Rev. B **80**, 125305 (2009); A. Petković and M. V. Milovanović, Phys. Rev. Lett. **98**, 066808 (2007).
[37]Within the local density approximation, Mn magnetization patterns appear also for higher QD occupancies (circular QDs and homogeneous Mn doping) [R. Abolfath, M. Korkusinski, T. Brabec, and P. Hawrylak, Phys. Rev. Lett. **108**, 247203 (2012)].
[38]K. Katayama, K. Miyajima, M. Ashida, and T. Itoh, J. Phys.: Condens. Matter **24**, 325801 (2012).
[39]I. Žutić, J. Fabian, and S. Das Sarma, Rev. Mod. Phys. **76**, 323 (2004).
[40]For $T = 0$ (full saturation), E_{PS} as well as the final-state (single-hole) energies are constant above B_0.
[41]M. A. Cusack, P. R. Briddon, and M. Jaros, Phys. Rev. B **56**, 4047 (1997); S. Raymond, X. Guo, J. L. Merz, and S. Fafard, *ibid.* **59**, 7624 (1999).
[42]To clarify whether the forbidden transitions are not due to low confinement symmetry [E. Siebert, T. Warming, A. Schliwa, E. Stock, M. Winkelnkemper, S. Rodt, and D. Bimberg, Phys. Rev. B **79**, 205321 (2009)], the experiment may be repeated at a temperature at which magnetic bipolarons no longer exist.
[43]L. W. Molenkamp (private communication); J. R. Maze *et al.*, Nature (London) **455**, 644 (2008).
[44]S. D. Bader, Rev. Mod. Phys. **78**, 1 (2006).
[45]B. Braunecker, P. Simon, and D. Loss, Phys. Rev. B **80**, 165119 (2009); P. Simon, B. Braunecker, and D. Loss, *ibid.* **77**, 045108 (2008).